Infiltration simulation model testing, for silty soil-water after Hortonian incident and settlement process

Stephanos D.V. Giakoumatos [1*], *Christina* Siontorou [1] and *Dimitrios* Sidiras [1]

[1] Laboratory of Simulation of Industrial Processes, Department of Industrial Management and Technology, School of Maritime and Industrial Studies, University of Piraeus, 80 Karaoli and Dimitriou, GR 18534, Piraeus, Greece

Abstract. Heavy rainfall incidents incur rapid topsoil swelling and runoff phenomena. Two models in lab scale testing, simulate top soil resuspension and settlement. The fitting of each model was tested, upon the lab scale observed values, under certain experimental conditions. In the experimental lab testing scenario, the fitting superiority of B-Z over T-B model is apparent. The superiority sustains, when all experimental values are included, along with all tested '*moving windows*' which correspond to truncated experimental values. The superiority is expressed by calculating the SEE value in all testing modes, thus, $SEE_{B\text{-}Z}<SEE_{T\text{-}B}$. The evolving sedimentation in mainly controlled by the water-glass wall effect and the wettability surface of packed materials.

1 Introduction

Soil water infiltration is a multi-stage process during which, in most cases, aquatic-based solution, enters the soil surface, under the effect of certain driving forces e.g. gravity, adhension/adsorption, capillary action etc., in deeper stratification.

Topsoil fertilizing to support intense crop cultivation and irrigation introduces the '*fertigation*' term, which denotes the soil enrichment with nutrients, primarily nitrogen, phosphorus and secondarily potassium to support high crop yield. Soil nutrients management plan is quite critical, so as to prevent diluted nitrogen surplus, as nitrates, to be diffused underground and reach aquifers. The humic fraction of the soil significantly regulates the fate of the ground nitrogen pool and controls the soil nitrification process, with important environmental outcomes such as groundwater nitrification, soil fertility, cation exchange capacity, and microbiota development. Infiltration/settlement action, though profoundly investigated in many scientific fields i.e. wastewater treatment and industrial processing, curve modelling is considered to be of relative low interest and cover a relatively narrow range of applications e.g. oilfield [1], polluted aquifers [2], mining processing [3], wastewater treatment plants [4].

During precipitation, rainwater receives impurities derived from agricultural/industrial activities, domestic poorly treated wastewater effluents. Diluted agents enter the ground and gradually reach the water table. In their route they undergo filtration, chemical reactions, ion-exchange, biochemical conversion, sedimentation, coagulation, flocculation, pore size swelling etc. [5]. Nitrogen pool, transform nitrogen to nitrate. The latter is leaching from the top soil zone to deeper layers. Nitrogen based fertilizers contribute to annual nitrogenous pollutants formation in different periods. Certain quantities are releasing and circulate to the hydrosphere [6].

Heavy rainfall incidents incur rapid topsoil swelling after persistent overland flow and runoff phenomena. Certain sedimentation models simulate soil water mixture compression in various incidents. In the present manuscript, two lab scale tested models, simulate compression/sedimentation phenomena, such as top soil resuspension and settlement. The present manuscript investigates the fitting of two settlement model formulas, after water and silty soil compression occurs and models' parameter response under various experimental conditions.

2 Sedimentation curves and water-soil particles compression zones

Forced chemical induced precipitation is a common practice to encounter industrial wastewater treatment plants and other industrial clarification processes. Thus, in mining activities, suspended particles dewatering is a common engineering practice [3]. Wastewater thickener facilities make use of such segregation [4].

Great effort was given over batch systems settling curves that interpretate settling phases '*moving window*' [7]. [8] introduced a *H(t)* compression and settling equation. [3] published a settling model to forecast the performance of batch sedimentation including certain sub-phases.

The 'jar test,' wherein suspended particles are let to settle for a duration dictated by their concentration and cohesiveness, is commonly employed to assess

* Corresponding author: sgiakoum@webmail.unipi.gr

sedimentation. Following sufficient sedimentation, the size distribution, the charge of the particles which is characteristic of their origin, and their uniformity exert a crucial influence in the resulted clarity. According to related literature, distinct zones known as '*settling zones*' occur (see **Fig. 1**). The starting concentration determines the evolution of the sludge '*blanket*' during the settling phase zones [9].

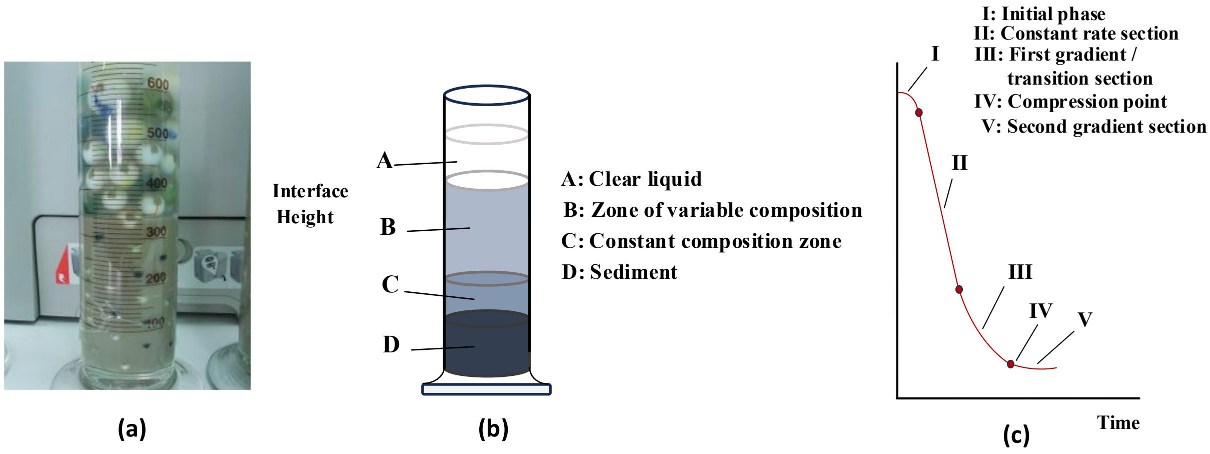

Fig. 1. (a) Settlement bands in a cylinder packed with glass spheres. Glass-packed material is slightly submerged beneath the water's surface. (b) Outlined settlement areas of suspended matter (c) Compression zones against time elapsed.

3 Two sedimentation models comparison

The [8] presented model, (Tchobanoglous and Burton model), is a first order kinetic model (eq. 1), that simulates adequately the sludge compression settling stage in wastewater treatment, known as compression '*type-4*'. According to the settling formula, is presumed that ongoing wastewater sludge compression process is proportional to (H-H_∞) quantity, where H denotes the suspension matter height for a given time (t) and H_∞ denotes the suspension height considering that $t \to \infty$. Thus:

$$\frac{dH}{dt} = -k \cdot (H - H_\infty) \quad (1)$$

or

$$\frac{dH}{(H - H_\infty)} = -k \cdot dt \quad (2)$$

and after the integration from $t_0 \to t$ and $H_0 \to H$ we obtain:

$$H = H_\infty + (H_0 - H_\infty) \cdot e^{-k \cdot (t - t_0)} \quad (3)$$

k (s^{-1}) parameter is constant for a given suspension. The linearized $y = a_o + a_1 \cdot x$ form of equation (1) is given below:

$$\ln \frac{H - H_\infty}{H^* - H} = \ln m - k \cdot t \quad (4)$$

A Symmetrical Reverse Sigmoid Model (SRSM) [10], (Batzias and Zervopoulou model), simulates with high explainability individual settling phases demonstrates a good fitting accuracy. According to SRSM function, in which the sedimentation is proportional to the product of the two distances i.e. (H^*-H) and (H-H_∞), the differential form of the sludge '*blanket*' height against time is presented as follows:

$$\frac{dH}{dt} = -k \cdot (H^* - H) \cdot (H - H_\infty) \quad (5)$$

$$\frac{dH}{(H^* - H) \cdot (H - H_\infty)} = -k \cdot dt \quad (6)$$

The integration from $t = 0$ to $t \to t$ and H=H_i to $H \to H$, gives the 4-parameter model (eq. 7) where H^*, H_∞ m, k are parameters where (m>0, k>0), k (min^{-1}) and m (dimensionless). H_∞ denotes the state when no more compression is taking place. H^* signifies the time when the soil water '*blanket*' stands at the highest interface level i.e. t=t_0 before settlement commences.

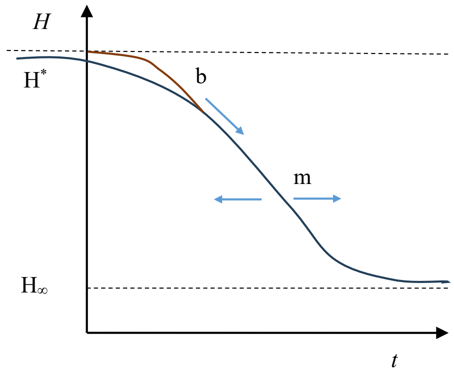

Fig. 2. SRSM curve. Brown colored line denotes the experimental curve at the initial particle compression stage.

$$H = H^* - \frac{H^* - H_\infty}{(1 + m * e^{-k*t})} \quad (7)$$

The linearized form of equation (7) is given below:

$$ln\left(\frac{H - H_\infty}{H_0 - H_\infty}\right) = -k * t + k * t_0 \quad (8)$$

Theoretically, for t→-∞, *H*→-∞, which yields H^*, and for t→∞, we obtain H_∞. Consequently, H^* and H_∞ define the zone of the curve to be drawn (upper limit zone and lower limit zone, respectively) by identifying the values that horizontally intercept the vertical axis. However, H^* has no physical meaning. In the inverse sigmoid equation, b parameter represents the speed of the curve line moving (see Fig. 2) graph. The parameter m is a line curvature controller and *H* denotes the silt suspension column height at a certain time t. Notably, when (H^*-*H*) is constant, i.e., within the time range, Tchobanoglous and Burton's settling formula (T-B) is just a special case of Batzias and Zervopoulou's (B-Z) sigmoid model.

4 Materials and methods

Lab scale experiments were conducted by using large glass cylinders with three different inner diameters. Before being poured into the glass cylinder, a predetermined mass dosimetry of silt and a premeasured volume of tap water were well mixed in a small container. Prior to the compression beginning, the water volume (x mL) to be poured into each different cylinder, was determined by making use of the following formula, where r_1, r_2 are the internal radii of two different cylinder sizes (eq. 9).

$$\frac{500mL}{{r_1}^2} = \frac{x(mL)}{{r_2}^2} \quad (9)$$

The packing material, comprised of identical glass sphere of known diameter, was placed carefully in the cylinders in an optimized way i.e. completely submerged in the tap water-silt mixture targeting effective porosity maximization in the filled-up cylinder. The effective porosity defined as the volume of voids in a predefined mass of rock or soil that can be drained by gravity divided by the volume of the mass under testing, is properly defined by (ASTM D653-20) standardization. The mixture then is allowed to rest. Strong indication that compression had almost finished was obtained when three consecutive identical readings of the compressed zone height were obtained by measuring and recording the height of the compressed suspended silt '*blanket*' every four minutes.

Three distinct configurations of the cylinder and tap water silt mixture were used for each experiment. Each configuration corresponds to an independent variable i.e. cylinder inner diameter, (i.e. 1- & 2-Liter glass column of diameter of 6.7 and 8.2 cm respectively, 2-Liter plexiglass column with a diameter equals 5.35cm), effective porosity (Φ_e), silt-water concentration (i.e. 30, 50, 100g/L). The column was prepared either unpacked, viz only silt-water interface in glass and plexiglass walls either packed with small spheres, (d=1.6 cm) and large spheres (d=2.5 cm).

The cylinder's packed or unpacked silt-water interface, mimics the settling and infiltration of particles during heavy rains. Given that the material underwent appropriate mesh testing, the brown fine-grained silt exhibits particle homogeneity.

5 Model parameters' estimation and statistical analysis

In order to carry out the fitting optimization of parameters k, H_0, H_∞, t_0 of (eq. 3) and m, b, H_0, H_∞, parameters of (eq. 7), linearization stage (eq. 4 & 8) of both functions is going to provide proper initial values so as to run the non-linear regression routine. The recording of experimental data provides information to proceed with the calculation of initial guesses of k, m and b parameters of (eq. 3) and (eq. 6). The initial parameter estimation serves as an initial estimation approach, by means of least square regression procedure to identify line slope and y-axis intercept after linearization occurs. Standard Error of Estimate (SEE) was reported after non-linear regression analysis was conducted in a variety of experimental setups (eq. 10).

$$SEE = \sqrt{\frac{\sum\left(y_{exp} - y_{est}\right)^2}{N - p}} \quad (10)$$

The well-known Generalized Reduced Gradient (GRG) approach serves for the obtained convergence. The dependent variables are optimized until a minimization is computed by the reduced gradient, which signifies the obtained convergence [11-12].

Table 1 presents the experimental data and computational results for a representative experimental run, corresponding to tap water with a silt concentration of 100 $g \cdot L^{-1}$, using a large cylinder packed with large spherical material. Curve fitting of T-B and B-Z settling models were tested by simulating in the lab, the water infiltration in silty soils after Hortonian overland flow.

6 Discussion

When appropriate porous terrain is preferred, infiltration occurs during Hortonian occurrences, followed by successive phases i.e. suspension, sedimentation, compression, infiltration phenomena at topsoil level. Since multiple partial processes occur simultaneously, it is not possible to identify and quantify the parameters of the corresponding simulation model a priori. Water fate into the soil is directly impacted by the soil structure, which includes the arrangement of soil particles and the texture of the soil (sandy, silt-rich, mostly silty, loamy, etc.). Therefore, in comparison to compacted or poorly structured soils, well-structured soils with bigger aggregates/organic colloids, a specific degree of hydrophobicity that is controlled by the chemical affinity, correct texture, and water content promote faster penetration [13]. Additionally, drainage/runoff phenomena that result in Hortonian events are influenced by the distribution of pore sizes and the features of the terrain.

Compared to other more gritty sandy soils, silty soils have a smooth texture and prefer to retain moisture and nutrients because their fine particles are usually larger than clay but smaller than sand. They have a large surface area that allows them to retain vital nutrients in the water phase, particularly during irrigation, [14], and they can hold and exchange positively charged ions like calcium, magnesium, and potassium due to their moderate cation exchange capacity (CEC). Since their surfaces are typically negatively charged, they can draw in and retain positively charged water molecules, such as hydrogen ions. In silty soils, organic matter (humus) can also increase the chemical affinity and soil fertility by improving the soil's overall ability to retain water and nutrients.

Silty soils may retain moisture longer as a result of this attraction, increasing their vulnerability to compaction and waterlogging. Additionally, this type of soil has a high capillary activity, which promotes moisture retention. This characteristic makes it possible to get water from deeper soil layers, which supports plant growth. Silty soils are susceptible to erosion when saturated. Silty soils are susceptible to runoff occurrences because the tiny particles are quickly removed by forced water flow [15].

In Table 1, SEE values are demonstrated as a result of the preceded calculation upon a selected experimental scenario. That is, tap water with a silt concentration of 100 $g \cdot L^{-1}$, using a large cylinder with an internal diameter of 8.2 cm, packed with large spherical material (d_{sph} = 1.6 cm). This configuration was chosen as the most representative for the research purposes. The continuous compression phenomena are greatly impacted by the interaction between soil and fine-granular silt., which also prevents the evolving compression. When it comes to sedimentation and compression, silt-water forces are very important. The progressive sedimentation is easily controlled by gravity, the water-glass wall effect, and the effective porosity of packed materials.

Glass wall columns that are packed could be used to simply model infiltration following Hortonian phenomena that take place over soil types that are dominated by silt or sand. The observed (*H* vs *t*) curve is presented in Fig. 3 as the experimental value pool for models' evaluation. In Fig. 3(a) no truncation of experimental values is attempted for the fitting of the two tested models i.e. T-B and B-Z settling models. Truncations of the observed values were tested over the models' testing, see Fig. 3(b)-3(e).

In experimental configuration testing, the fitting superiority of B-Z model over T-B model is apparent for the observed values (truncated of not). The B-Z model corresponds better, overall, as expressed by constant lower SEE values (i.e. $SEE_{B\text{-}Z}<SEE_{T\text{-}B}$), an indication of better model equation fitting (see Table 1 and Fig. 1). Both models were tested with different number of initial truncated observed values, viz 3,6,9,12, functioning as a '*moving window*' fitting curve to verify fitness capability over individual compression zones. The plot of residual analysis without truncated values, see Fig. 1(f), deciphers that B-Z model lies closer to the X-axis, therefore, fits better to the observed experimental compression curve. Furthermore, residual difference over compression elapsed time is depicted in Fig. 1(g). As a gauge of local goodness of fitting, or how closely each estimated value matches the corresponding experimental result, the Fig. 1(h) specifies the absolute values of the corresponding residuals. During the compression development, a negative difference shows that the B-Z model is (at least locally) superior to the T-B model.

Table 1. Tested models parameter calculation for experimental mode i.e. tap water-silt concentration $100 g.L^{-1}$, large cylinder used, large spheres packed material

	T-B model				
Parameter	no truncation	3-truncated values	6-truncated values	9-truncated values	12-truncated values
H_o (cm)	30.977	30.729	30.4420	30.079	29.601
H_∞ (cm)	15.680	15.680	15.680	15.680	15.680
t_o (min)	25.548	34.541	43.3804	52.282	61.254
k (s^{-1})	0.008129	0.008901	0.009760	0.01071	0.01173
SEE	1.6507	1.5188	1.3695	1.2232	1.0968
Parameter	**B-Z model**				
H_o (cm)	30.9774	30.7290	30.442	29.868	29.601
H_∞ (cm)	15.6798	15.6799	15.680	15.680	15.680
t_o (min)	0	12	24	36	48
k (s^{-1})	0.02887	0.0294	0.03010	0.0315	0.0320
m	35.4506	39.7359	45.680	60.2768	67.0788
SEE	0.3718	0.3742	0.3880	0.4123	0.3898

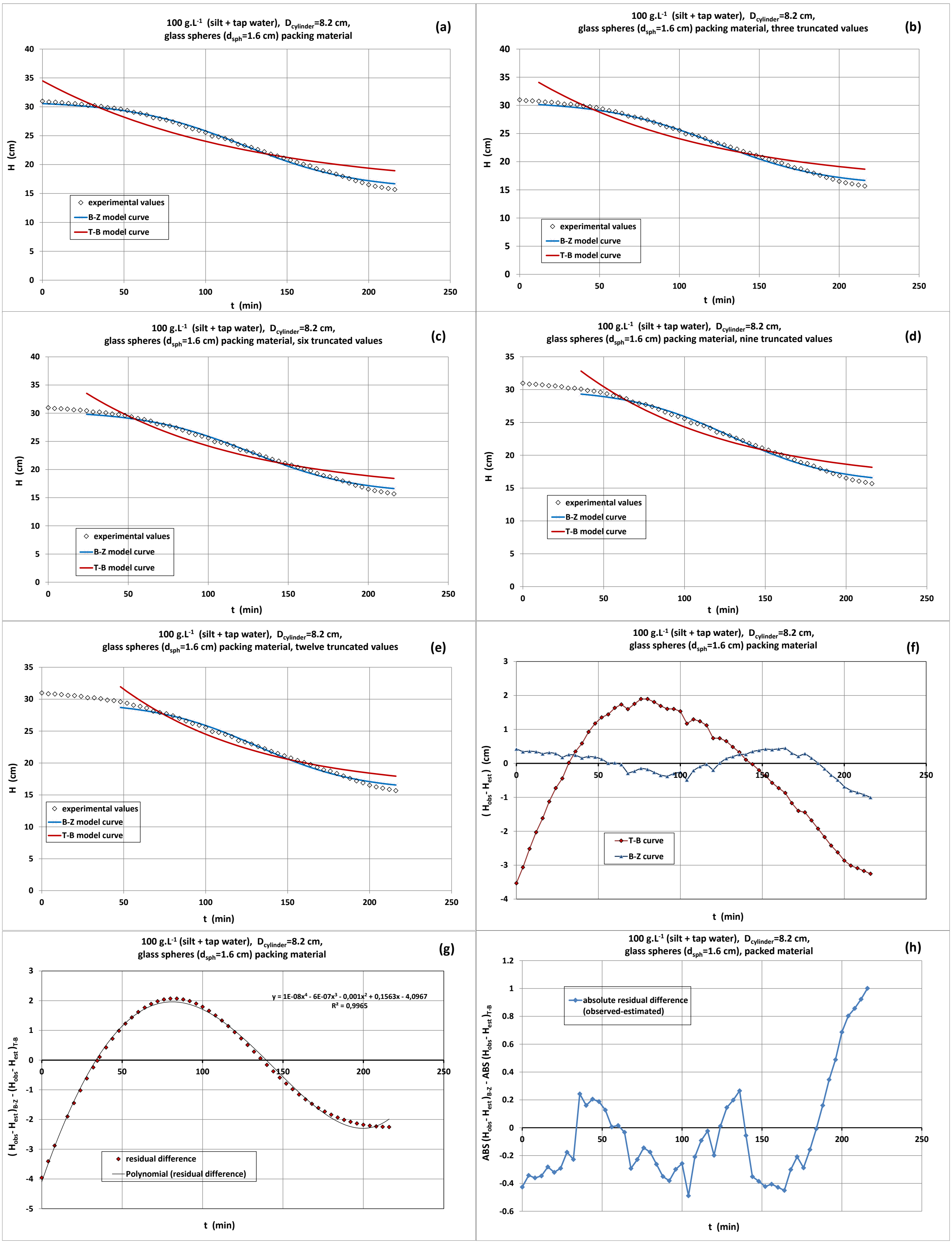

Fig. 3. Dependent parameters estimation and fitting curves in a specified experimental configuration

7 Conclusion

Glass wall packed/non-packed columns could simulate simplistically Hortonian infiltration phenomena over silty dominated topsoil with smooth texture characteristics and certain coarse-grained elements in the soil.

The absence of organic matter (humus) in lab silty soils, deprive the compression, infiltration process from chemical affinity and biochemical interactions resulting from vivid biological activity that might retain moisture longer, making them prone to compaction and waterlogging. High capillary action favors moisture retention. Predominant fine particles in soils are easily dislodged by forced water movement, making areas with high silty content vulnerable to runoff incidents.

Lab evolving phenomena during the infiltration process, by using glass/plexiglass tubes such as capillary action and wetting front propagation, are more easily tracked down visually and isolated for further analysis taking advantage of the glass transparency. In order to focus on the impacts of packed material diameter and packing intensity, which have a considerable impact on penetration rates, the utilized glass spheres exclude variables that are difficult to isolate and monitor.

The compression phenomena are greatly impacted by the fine-granular silt-soil interaction, which also prevents the evolving compression. During compression, silt crystal-water forces are quite important. Our straightforward method controls the evolving sedimentation through the water-glass wall effect and the wettability surface of packed materials. The amount of time needed to reach a stable soil-water level interaction increases with the predetermined silt water concentration.

The fitting superiority of B-Z over T-B model is apparent in a selected lab running experimental scenario. The superiority sustains, when all experimental values are included, along with all tested '*moving windows*' which correspond to truncated experimental values. The superiority is demonstrated by calculating the SEE value in all testing modes, thus, $SEE_{B\text{-}Z} < SEE_{T\text{-}B}$.

Acknowledgements: This work has been partly supported by the University of Piraeus Research Center.

Fundings: This research received no external funding
Data availability statement: Upon request

Author contribution statement: Writing—original draft preparation S.D.V.G.; writing—review and editing, S.D.V.G., C.S. and D.S., Visualization S.D.V.G., Methodology S.D.V.G. and S.S., Investigation S.D.V.G., supervision, C.S. and D.S.

References

1. H. Chen, Z. Ren, R. Liu, F. Liu, G. Zhang, Contamination characteristics and mechanism of groundwater movement in an oilfield in Northeast China. Earth Sci. Front. **15** (4), 178–185 (2008). https://doi.org/10.1016/S1872-5791(08)60051-2
2. K.P. Sedlazeck, D. Höllen, P. Müller, R. Mischitz, R. Gieré, Mineralogical and geochemical characterization of a chromium contamination in an aquifer - A combined analytical and modeling approach. Appl. Geochem. **87**, 44–56 (2017). https:// doi.org/10.1016/j.apgeochem.2017.10.011
3. L. Zhang, A. Wu, H. Wang, L. Wang, Representation of Batch Settling via Fitting a Logistic Function. Miner. Eng. **128**, 160–67 (2018). https://doi.org/10.1016/j.mineng.2018.08.039
4. R. Hasanzadeh, J.S. Amin, B.A. Souraki, O. Mohammadzadeh, S. Zendehboudi, Reliable Tools to Forecast Sludge Settling Behavior: Empirical Modeling. Energies **16** (2), 963 (2023). https://doi.org/10.3390/en16020963
5. S.D.V. Giakoumatos, C. Siontorou, D. Sidiras, An Extensive Review of Leaching Models for the Forecasting and Integrated Management of Surface and Groundwater Quality. Water **16**, 3348 (2024). https://doi.org/10.3390/w1623334
6. D.S. Jenkinson, L.C. Parry, The nitrogen cycle in the Broadbalk wheat experiment: a model for the turnover of nitrogen through the soil microbial biomass. Soil Biol. Biochem. **21**, (4) 535–541 (1989). https://doi.org/10.1016/0038-0717(89)90127-2
7. P. Grassia, S.P. Usher, P.J. Scales, A simplified parameter extraction technique using batch settling data to estimate suspension material properties in dewatering applications, Chem. Eng. Sci. **63**, (7), 1971-1986 (2008). https://doi.org/10.1016/j.ces.2007.12.025
8. G. Tchobanoglous, F.L. Burton, Wastewater Engineering, Treatment Disposal and Reuse, 3rd edition, Metcalf & Eddy Inc., McGraw & Hill, Inc. international 1991.
9. A. Vanderhasselt, P.A. Vanrolleghem, Estimation of Sludge Sedimentation Parameters from Single Batch Settling Curves. Water Res., **34**, (2) 395–406 (2000). https://doi.org/10.1016/S0043-1354(99)00158-X
10. F.A. Batzias, S.P. Zervopoulou, Simulating the behavior of seawater contaminated with oil spill and chemical dispersant when approaching a windy shore. Inter. J. Arts Sci. 7, (3) 271–282 (2014). (access 12 June 2025), available on https://universitypublications.net/ijas/0703/pdf/P4RS414.pdf
11. L.S. Lasdon, R.L, Fox, M.W. Ratner, Nonlinear optimization using the generalized reduced gradient method. Revue française d'automatique, informatique, recherche operationnelle. Rech. Oper. **8**, (V3), 73–103 (1974).
12. J.S. Arora, Chapter 13 - more on numerical methods for constrained optimum design. Introduction to Optimum Design (Third Edition). (Academic Press, Elsevier, pp. 533–573, U.K., 2012). https://mu.menofia.edu.eg/PrtlFiles/Staff/1045/Portal/Files/Introduction%20to%20Optimum%20Design,%203nd%20Ed(3).pdf

13. C. Basset, M.A. Najm, T. Ghezzehei, X. Hao, A. Daccache, How does soil structure affect water infiltration? A meta-data systematic review, Soil Till. Res. **226**, 105577 (2023). https://doi.org/10.1016/j.still.2022.105577
14. H.J.M. Morrás, Mineralogy and cation exchange capacity of the fine silt fraction in two soils from the southern Chaco Region (Argentina). Geoderma, **64**, (3–4), 281-295 (1995). https://doi.org/10.1016/0016-7061(94)00024-5
15. U. Buczko, O. Bens, R.F. Hüttl, Tillage Effects on Hydraulic Properties and Macroporosity in Silty and Sandy Soils. Soil Sci. Soc. Am. J., **70**, 1998-2007 (2006). https://doi.org/10.2136/sssaj2006.0046